Unifying microscopic mechanism for pressure and cold denaturations of proteins

Cristiano L. Dias
Fachbereich Physik, Freie Universität Berlin, Arnimalle 14, 14195 Berlin, Germany
(Dated: May 29, 2012)

We study the stability of globular proteins as a function of temperature and pressure through NPT simulations of a coarse-grained model. We reproduce the elliptical stability of proteins and highlight a unifying microscopic mechanism for pressure and cold denaturations. The mechanism involves the solvation of non-polar residues with a thin layer of water. These solvated states have lower volume and lower hydrogen-bond energy compared to other conformations of non-polar solutes. Hence, these solvated states are favorable at high pressure and low temperature, and they facilitate protein unfolding under these thermodynamical conditions.

Native protein conformations are only stable within a narrow range of thermodynamical conditions, unfolding at low and high temperatures as well as under pressure [1–6]. Unfolding at high temperatures is commonly exemplified by albumin (the main constituent of egg white), which denatures irreversibly when heated conveying color and texture to boiled eggs. Low-temperature unfolding, i.e., cold denaturation, has been empirically verified for many proteins [7–9], and its understanding is emerging as a consequence of the states assumed by *shell water*, i.e., water molecules in the vicinity of the protein [10–17, 17–20]. In 1914, Bridgman first demonstrated pressure denaturation by "cooking" an egg using pressure (5000-12,000 atm) solely (no heat) [21]. While high temperature unfolding is well understood, the microscopic mechanisms for the other two transitions are still under debate despite recent progress [11, 22, 23]. Understanding the microscopic forces leading to these transitions is crucial to grasp the limits under which proteins can function in cells and to design new stable folds.

Hydrophobic interactions are linked to protein stability [24–27]. In particular, a decrease in the strength of hydrophobic interactions upon cooling has been associated with *cold denaturation*. At the molecular level, this is due to the stronger hydrogen-bonding capacity of shell water compared to bulk water [28–30]. Hence, unfolding, which increases the amount of shell water in the system, leads to a decrease in hydrogen-bond energy (enthalpy) and is therefore favored at low temperatures [11]. Hydrophobic interactions have also been associated with *pressure denaturation* as simulations showed that solvated configurations of non-polar compounds became increasingly more favorable with increasing pressure [31–33]. Pressure, therefore, squeezes water molecules inside the protein core, solvating hydrophobic residues with a single layer of water [31, 34–36]. However, hydrophobicity cannot explain *volume changes* measured during protein unfolding [37]. They are either positive [40] or negative [39, 40] at small pressures, and invariably negative at high pressures [41]. In contrast, the transfer of non-polar solutes (e.g., methane) from a nonaqueous hydrophobic solvent to water accounts for a large negative volume change at low pressure [42–46]. This volume change increases with applied pressure becoming positive at approximately 1500–2000 atm [46]. Thus, the *liquid hydrocarbon model*, which describes unfolding by the transfer of non-polar residues into bulk water, gives not only wrong magnitudes for volume changes of unfolding but also a wrong sign [47–49].

This discrepancy could be explained by the fact that the liquid hydrocarbon model does not consider the connectivity between non-polar residues in proteins [24]. In fact, geometry imposes constraints on allowed distances between residues along secondary protein structures (β-sheets and α-helices). These constraints inhibit non-polar residues from being completely solvated (bulk hydrophobicity) and in β-sheets favor *solvent-separated configurations (ssc)*, i.e., configurations in which these residues are separated from each other by a single layer of water molecules [50–53, 79]. Solvation properties of ssc differ from those of non-polar aggregation predicted on the basis of bulk hydrophobicity: ssc formation (i) is driven by enthalpy (instead of entropy), (ii) becomes favorable (instead of unfavorable) with decreasing temperature and increasing pressure [54–56], and (iii) has a negative volume compared to other configurations [57]. In light of these results, a possible scenario for pressure and cold denaturation is that tertiary hydrophobic contacts disrupt in favor of ssc. In this process, proteins are released from their biological functions, and at high pressures and/or low temperatures, unfolded structures retain part of their native secondary structures. This mechanism agrees with experimental results that have shown unfolded states at high pressure [4] and low temperature [58] to remain globular, although swelled, and to retain some secondary structures [38, 59].

To test the suggested scenario we use a bead-spring model to mimic hydrophobic proteins and the two-dimensional Mercedes-Benz model (MB) for water [60–62]. Two [11, 63–65] and three [55, 60, 66–69] dimensional versions of the MB model have been shown to reproduce the properties of water and the solvation of small compounds. We show that the elliptical stability of proteins emerges naturally as a function of pressure and temperature. Furthermore, the volume of the system and the hydrogen-bond energy of shell water decrease when the protein unfolds at high pressure and/or low temperature. We identify ssc formation as the main cause of this phenomena and rationalize cold and pressure denaturation in terms of the *non-polar dimer* model. The proposed

ϵ_h	R_h	σ	ϵ_{ww}	σ_{ww}	ϵ_{mm}	σ_{mm}	ϵ_{wm}	σ_{wm}	K_s	R_s
1	1	0.085	0.1	0.7	0.375	1.1	0.1	0.9	282.644	2

TABLE I: Parameters of the model.

unifying mechanism is possible because ssc formation accounts for an overall decrease in volume [57] and enthalpy [54–56, 63].

Here, we summarize the main features of the MB forcefield and refer the readers to reference 61 for a detailed mathematical description. The interaction between MB molecules occurs through a combination of Van der Waals and hydrogen-bond energies. Van der Waals interactions are described by 12-6 Lennard–Jones potentials with binding energy ϵ_{ww} and distance parameter σ_{ww}. To account for hydrogen-bonds, MB molecules are assigned three rigid arms resembling the logo of a Mercedes-Benz car. An hydrogen-bond between molecules i and j is described by the product of three Gaussian functions of width σ. These functions are determined such that they favor configurations in which the distance between molecules i and j is R_h and one arm of both molecule i and j is aligned with the line joining the two centers of mass. When these conditions are satisfied, the hydrogen-bond energy is -ϵ_H. The mass of water is set to one and 1/10 of the total mass is set at each arm's extremity at a distance $R_{arm} = 0.36\ R_h$ from the center of mass [11, 70].

The protein is modelled by beads attached by springs with equilibrium distance R_s and stiffness K_s. Non-adjacent beads along the backbone are characterized by Lennard-Jones potentials with binding energy ϵ_{mm} and distance σ_{mm}. Interactions between beads and MB molecules are described by Lenard-Jones potentials with binding energy ϵ_{mw} and distance σ_{mw}. Beads are set to be ten times heavier than water molecules.

All Lennard-Jones potentials are shifted such that the force becomes zero at the cut-off distance $R_{cutoff} = 2.5\ R_h$ [71]. The set of parameters used in this work (see table I) have been shown to reproduce different properties of water and its solvation properties [11, 61, 63].

Energies, distances, and time are given in units of ϵ_h, R_h, and $\tau_o = \sqrt{\epsilon_{ww}/M_w\sigma_{ww}^2}$, respectively. Pressure is given in units of ϵ_h/R_h^2. In this work, we perform Langevin-dynamics in the isothermal-isobaric ensemble [72] using a friction constant of $\gamma^{-1} = 0.93\ \tau_o$. We use periodic boundary conditions in boxes packed with a 20-bead long protein and 492 MB molecules. Starting from random initial conditions, we perform simulations at six different pressures: 0.05, 0.10, 0.15, 0.20, 0.25, and 0.30. Under each pressure, the sample was probed at eight different temperatures: 0.17, 0.18, 0.19, 0.20, 0.21, 0.22, 0.23, and 0.24. The first 100,000 units of time were discarded, and statistics were gathered along the next 400,000 units of time. We used 25 samples for P = 0.05, 0.10 and 0.15, and 99 samples for P = 0.20, 0.25, and 0.30.

Fig. 1(a) shows the dependence of the average radius of gyration $\langle R_{gy}\rangle$ on temperature at three different pressures. At all pressures, $\langle R_{gy}\rangle$ has a parabolic-like shape indicating that the protein model is maximally compact at intermediate temperatures (∼0.20) and that it extends gradually as the system is heated up or cooled down [73]. Furthermore, as shown in Fig. 1(a), increasing pressure increases the temperature at which the protein is maximally compact (minimum $\langle R_{gy}\rangle$) [74]. Each colored square in Fig. 1(b) represents the average radius of gyration of a simulated thermodynamic condition. Contour lines along three values of $\langle R_{gy}\rangle$ are also shown. The compactness of the protein remains constant along contour lines, and the protein swells as $\langle R_{gy}\rangle$ increases. States of similar compactness have an elliptical dependence on temperature and pressure. This characterizes the stability of real proteins [1–3] and allows for heat, cold, and pressure denaturations, which are indicated by arrows in Fig. 1.

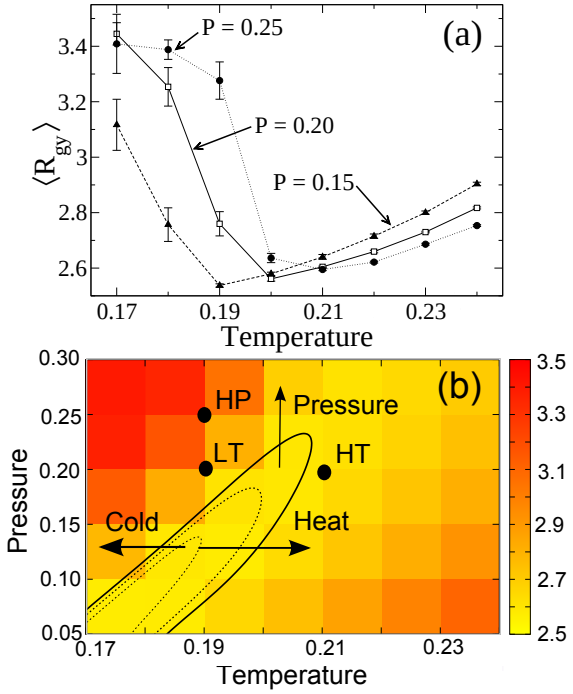

FIG. 1: (Color online) Stability of a hydrophobic protein in the pressure × temperature plane. (a) Dependence of the average radius of gyration on temperature at three different pressures. Error bars were computed using the block average method [76]. (b) Each colored square represents the average radius of gyration of a simulated thermodynamic condition. Contour lines are shown along $\langle R_{gy}\rangle = 2.55$ (dotted line), $\langle R_{gy}\rangle = 2.58$ (dashed line), and $\langle R_{gy}\rangle = 2.60$ (full line). Arrows show how globule-like configurations of the protein are destabilized through heat, pressure, and cold temperatures. High Pressure (HP), Low Temperature (LT), and High Temperature (HT) points are highlighted. They correspond to P = 0.25 and T = 0.19, P = 0.20 and T = 0.19, and P = 0.20 and T = 0.21, respectively.

According to Le Chatelier's principle, increasing pressure favors configurations that occupy a small space while decreasing temperature favors low enthalpic configurations. Since these pressure and temperature changes fa-

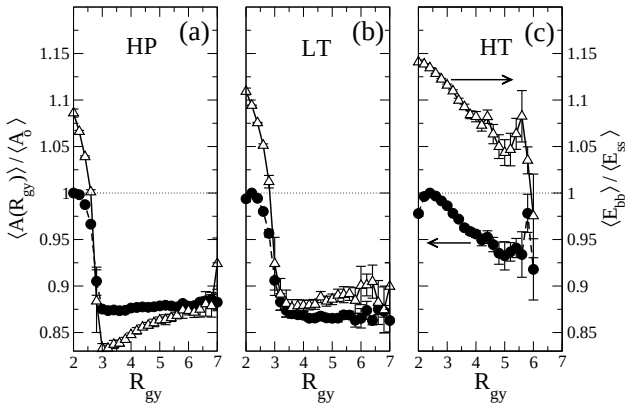

FIG. 2: Relative changes in area (circles) and hydrogen-bond energies (triangles) upon unfolding at different pressures and temperatures. $\langle A(R_{\rm gy})\rangle$ is the Voronoï volume of shell water plus protein per molecule averaged over configurations having $R_{\rm gy}$ as the radius of gyration of the protein. $\langle A_o\rangle$ is the maximum in $\langle A(R_{\rm gy})\rangle$. $\langle E_{bb}(R_{\rm gy})\rangle$ and $\langle E_{ss}(R_{\rm gy})\rangle$ are the hydrogen-bond energies between two bulk and two shell MB molecules, respectively, averaged over protein configurations characterized by $R_{\rm gy}$. High Pressure (HP), Low Temperature (LT) and High Temperature (HT) conditions are defined in Fig. 1. Error bars were computed using the block average method [76].

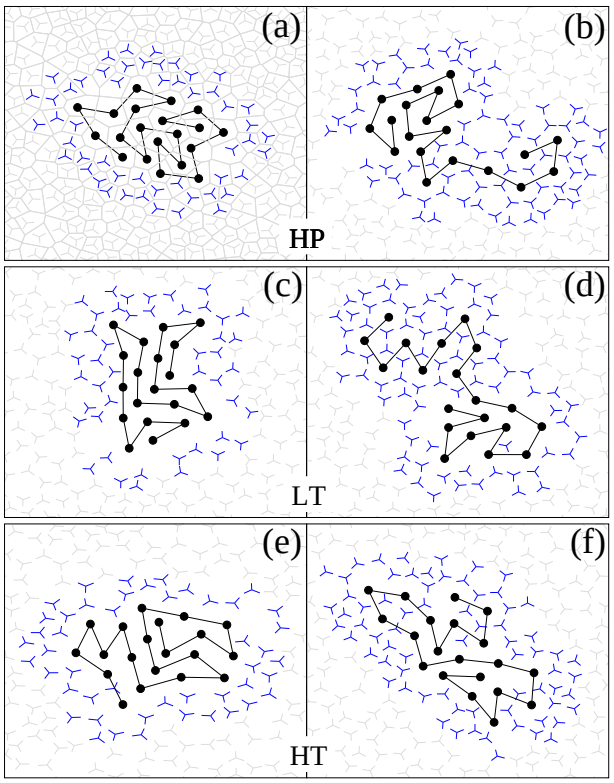

FIG. 3: (Color online) Compact (left panels) and extended (right) configurations of the hydrophobic protein at different temperatures and pressures. The Voronoï diagram, used to compute area, is illustrated in panel (a). The radius of gyration of these sample configurations are 2.18 (a), 3.06 (b), 2.45 (c), 3.31 (d), 2.26 (e), and 2.90 (f). Shell water is shown in blue. High Pressure (HP), Low Temperature (LT) and High Temperature (HT) conditions are defined in Fig. 1.

vor unfolded states (see Fig. 1), extended protein configurations should have a low area and a low enthalpy. This is verified from Fig. 2, which shows the dependence of Voronoï areas and hydrogen-bond energies on the radius of gyration of the protein at different pressures and temperatures. In Fig 2, $\langle A(R_{\rm gy})\rangle$ corresponds to the average Voronoï area [77] per molecule of protein plus shell water. We define shell water as being all MB molecules that are within a distance of 2.5 (in units of R_h) from the protein. A Voronoï tessellation is illustrated in Fig. 3(a). Voronoï areas of bulk water do not change significantly during unfolding, and therefore, they are not used in the calculation of $\langle A(R_{\rm gy})\rangle$. Furthermore, to compare changes in area at different pressures and temperatures, $\langle A(R_{\rm gy})\rangle$ is normalized using the largest average area $\langle A_o\rangle$ under the given thermodynamic conditions. At low temperatures, the unfolding of the protein leads to a sharp decrease in the space occupied by the system (panels a and b). At higher temperature, panel (c), unfolding accounts for a timid space contraction. Hence, increasing pressure at both high and low temperatures will favor protein unfolding because this leads to smaller areas, however, *space contraction during unfolding is more pronounced at low temperature and/or high pressure.*

Fig. 2 shows a decrease in enthalpy that occurs upon unfolding at low temperatures. We compute the hydrogen-bond energies involving bulk water E_{bb} and shell water E_{ss}, and we average these quantities over protein conformations that have the same radius of gyration. Fig. 2 shows the ratio between these quantities: $\langle E_{\rm bb}\rangle/\langle E_{\rm ss}\rangle$. At all temperatures, $\langle E_{\rm ss}\rangle$ is less favorable than $\langle E_{\rm bb}\rangle$ when the protein is folded (small $\langle R_{\rm gy}\rangle$). However, this trend changes abruptly when the protein unfolds (large values of $\langle R_{\rm gy}\rangle$) at low temperatures and high pressure (panels a and b): $\langle E_{\rm bb}\rangle/\langle E_{\rm ss}\rangle < 1$. Hence, *it is enthalpically favorable to unfold the protein at low temperatures and high pressures* because this increases the number of shell water molecules in the system that have lower hydrogen-bond energies than bulk water molecules. On the other hand shell water molecules do not form better hydrogen-bonds than bulk water molecules upon unfolding at high temperature (panel c). Hence, there is no enthalpic advantage to unfold proteins at high temperature.

Fig. 3 shows the characteristic configurations of compact (left column) and extended (right column) states of the hydrophobic protein at different conditions: HP (panels a and b), LT (panels c and d), and HT (panels e and f). Under every condition, folded protein configurations are characterized by shell-water molecules that have at least one unsaturated hydrogen-bond arm pointing towards the protein (panels a, c, and e). This explains why $\langle E_{bb}\rangle/\langle E_{ss}\rangle > 1$ for the low values of R_{gy} in Fig. 2. When proteins unfold at low temperatures and high pressures (panels b and d), shell-water molecules

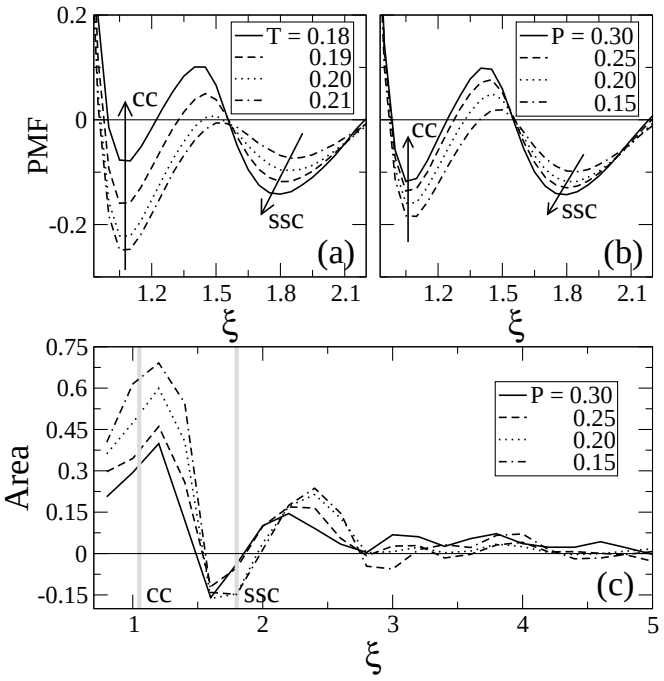

FIG. 4: Dependence of the Potential of Mean Force (PMF) on temperature (a) and pressure (b) as a function of dimer distance ξ. Changes in the PMF at contact-configurations (cc) and solvent-separated-configurations (ssc) are indicated by arrows. Dependence of area on dimer distance (ξ) at different pressures (c). Positions of cc and ssc are indicated by the vertical gray line.

form *clathrate* (cage-like) structures around residues at distances corresponding to *ssc*. In these conformations, all water hydrogen-bond arms are saturated. This explains why $\langle E_{bb}\rangle/\langle E_{ss}\rangle < 1$ for the large values of R_{gy} in Fig. 2(a-b). Cage-like structures are also present in unfolded protein conformations at high temperatures (panel f) but they occur mostly at residue distances different from ssc. Hence, most cages are incomplete with dangling hydrogen-bond arms left in the protein interior. This explains why $\langle E_{bb}\rangle/\langle E_{ss}\rangle > 1$ for the high values of R_{gy} in Fig. 2(c).

Hence, ssc is common to both cold and pressure denaturations. To study its properties, we observe the potential of mean force (PMF) of two non-polar solutes as a function of their distances (ξ) at different temperatures (Fig. 4(a)) and pressures (Fig. 4(b)). The PMF corresponds to the free energy required to bring the two solutes from an infinite distance to a distance ξ. In this study, the two solutes (defined by $\sigma_{mm} = 1.1$ and $\epsilon_{mm} = 0.2$) are immersed in 254 MB molecules, and NPT Langevin-dynamics are performed to compute their radial-distribution function ($\rho(\xi)$). The PMF is given as: $\mathrm{PMF}(\xi) = -kT\log(\rho(\xi))$. The distances between solutes is preferred when they are in contact ($\xi \approx 1.05$) and solvent-separated ($\xi \approx 1.8$) [78]. As temperature decreases (panel a), the PMF at cc increases while the PMF at ssc decreases. In other words, cc is destabilized in favor of ssc when the system is cooled down. These results have also been reported in simulations using atomistic water models [54, 56] and the MB model [55, 63]. A similar trend is also observed in panel b which shows that pressure destabilizes cc in favor of ssc. This result agrees qualitatively with NVT simulations using SPC/E [31], TIP3P [32] water models, and NPT simulations using TIP4P water models [79]. Panel (c) shows that the area occupied by the whole system depends on the distance between solutes. Under each pressure, the system occupies a smaller space when the solutes are at ssc. This result again agrees with extensive simulations using the TIP4P water model [57] and with simulations using the 2DMB model reported by another group at P = 0.19 [63].

In summary, we have shown that hydrophobic interactions can account for cold and pressure denaturations through formations of ssc. They explain the (i) elliptical stability of proteins as a function of pressure and temperature, (ii) decrease in the volume of the system during unfolding at elevated pressures, and (iii) decrease in enthalpy at low temperatures. Some secondary structures, e.g., β-sheets, are not expected to be disrupted by ssc because the distance between residues in ssc matches the periodicity of these conformations [50, 79]. Hence, our results support the view that pressure and cold denaturations are driven by the hydration of the non-polar protein core by a thin layer of water, leaving part of the secondary structures conserved. The proposed microscopic mechanism provides a unifying explanation for why proteins unfold at high pressure and low temperature. Although we studied protein stability in 2D, ssc is a general solvation state which has been observed in simulations of small non-polar compounds [78] and α-helical surfaces embedded in atomistic water models [27]. Furthermore, changes in the free energy (PMF) of ssc with respect to pressure and temperature in all-atomic 3D simulations are similar to the ones observed in Fig. 4 (a-b) [31, 54–56, 79]. Hence we expect ssc formation to contribute to protein unfolding at low temperature and high pressures in 3D systems.

I. ACKNOWLEDGMENT

C.L.D. would like to thank Martin Grant for hosting his staying at McGill University during the elaboration of this work, and Markus Miettinen for insightful discussions. This work was supported by the Volkswagen Foundation (C.L.D.). We are also grateful for the computing resources provided by SHARCNET (www.sharcnet.ca) of Compute Canada.

[1] S. A. Hawley, Biochemistry **10**, 2436 (1971).

[2] A. Zipp and W. Kauzmann, Biochemistry **12**, 4217

(1973).
[3] F. Meersman, C. M. Dobson, and K. Heremans, Chem. Soc. Rev. **35**, 908 (2006).
[4] G. Panick, G. J. A. Vidugiris, R. Malessa, G. Rapp, R. Winter, and C. A. Royer, Biochemistry **38**, 4157 (1999).
[5] R. Ravindra and R. Winter, ChemPhysChem **4**, 359 (2003).
[6] K. Heremans and L. Smeller, Biochimica et Biophysica Acta (BBA) - Protein Structure and Molecular Enzymology **1386**, 353 (1998).
[7] P. Privalov, Y. Griko, S. Venyaminov, and V. Kutyshenko, Journal of Molecular Biology **190**, 487 (1986).
[8] Y. V. Griko, P. L. Privalov, J. M. Sturtevant, and V. SYu, Proceedings of the National Academy of Sciences **85**, 3343 (1988).
[9] P. L. Privalov, Critical Reviews in Biochemistry and Molecular Biology **25**, 281 (1990).
[10] C. L. Dias, T. Ala-Nissila, J. Wong-ekkabut, I. Vattulainen, M. Grant, and M. Karttunen, Cryobiology **60**, 91 (2010).
[11] C. L. Dias, T. Ala-Nissila, M. Karttunen, I. Vattulainen, and M. Grant, Physical Review Letters **100**, 118101 (2008).
[12] P. De Los Rios and G. Caldarelli, Physical Review E **62**, 8449 (2000).
[13] P. De Los Rios and G. Caldarelli, Physical Review E **63**, 031802 (2001).
[14] O. Collet, Europhysics Letters (EPL) **53**, 93 (2001).
[15] C. F. Lopez, R. K. Darst, and P. J. Rossky, J. Phys. Chem. B **112**, 5961 (2008).
[16] T. Yoshidome and M. Kinoshita, Physical Review E **79**, 030905 (2009).
[17] V. Bianco, S. Iskrov, and G. Franzese, Journal of Biological Physics (2011).
[18] P. Bruscolini and L. Casetti, Physical Review E **61**, R2208 (2000).
[19] S. V. Buldyrev, P. Kumar, S. Sastry, H. E. Stanley, and S. Weiner, J. Phys.: Condens. Matter **22**, 284109 (2010).
[20] H. Oshima, T. Yoshidome, K. ichi Amano, and M. Kinoshita, J. Chem. Phys. **131**, 205102 (2009).
[21] P. W. Bridgman, Journal of Biological Chemistry **19**, 511 (1914).
[22] J. Rouget, T. Aksel, J. Roche, J. Saldana, A. E. Garcia, D. Barrick, and C. A. Royer, J. Am. Chem. Soc. **133**, 6020 (2011).
[23] D. Paschek, S. Hempel, and A. E. Garca, Proceedings of the National Academy of Sciences **105**, 17754 (2008).
[24] K. A. Dill, Biochemistry **29**, 7133 (1990).
[25] W. Kauzmann, Advances in Protein Chemistry **14**, 1 (1959).
[26] H. Li, C. Tang, and N. S. Wingreen, Physical Review Letters **79**, 765 (1997).
[27] J. L. MacCallum, M. S. Moghaddam, H. Chan, and D. Tieleman, PNAS **104**, 6206 (2007).
[28] H. S. Frank and M. W. Evans, The Journal of Chemical Physics **13**, 507 (1945).
[29] N. Muller, Acc. Chem. Res. **23**, 23 (1990).
[30] K. A. T. Silverstein, A. D. J. Haymet, and K. A. Dill, The Journal of Chemical Physics **111**, 8000 (1999).
[31] G. Hummer, S. Garde, A. E. Garca, M. E. Paulaitis, and L. R. Pratt, Proceedings of the National Academy of Sciences **95**, 1552 (1998).
[32] T. Ghosh, A. E. Garca, and S. Garde, J. Am. Chem. Soc. **123**, 10997 (2001).
[33] T. Ghosh, A. E. Garca, and S. Garde, The Journal of Chemical Physics **116**, 2480 (2002).
[34] D. B. Kitchen, L. H. Reed, and R. M. Levy, Biochemistry **31**, 10083 (1992).
[35] A. Paliwal, D. Asthagiri, D. P. Bossev, and M. E. Paulaitis, Biophysical Journal **87**, 3479 (2008).
[36] N. Smolin and R. Winter, Biochimica et Biophysica Acta **1764**, 522 (2006).
[37] Since proteins are 5–10 times less compressible than water [38], these volume changes are small (less than 1% of the overall protein volume) [39].
[38] R. Winter, D. Lopes, S. Grudzielanek, and K. Vogtt, Journal of Non-Equilibrium Thermodynamics **32**, 41 (2007).
[39] J. Brandts, R. Oliveira, and C. Westort, Biochemistry **9**, 1038 (1970).
[40] H. Hinz, T. Vogl, and R. Meyer, Biophysical Chemistry **52**, 275 (1994).
[41] C. A. Royer, Biochimica et Biophysica Acta (BBA) - Protein Structure and Molecular Enzymology **1595**, 201 (2002).
[42] W. L. Masterton, The Journal of Chemical Physics **22**, 1830 (1954).
[43] H. S. M.E. Friedman, J. Phys. Chem. **69**, 3795 (1965).
[44] K. Gekko and H. Noguchi, Macromolecules **7**, 225 (1974).
[45] Y. Taniguchi and K. Suzuki, J. Phys. Chem. **87**, 5185 (1983).
[46] S. Sawamura, K. Kitamura, and Y. Taniguchi, J. Phys. Chem. **93**, 4931 (1989).
[47] T. V. Chalikian and K. J. Breslauer, Biopolymers **39**, 619 (1996).
[48] T. V. Chalikian, Annual Review of Biophysics and Biomolecular Structure **32**, 207 (2003).
[49] W. Kauzmann, Nature **325**, 763 (1987).
[50] C. L. Dias, M. Karttunen, and H. S. Chan, Physical Review E **84**, 041931 (2011).
[51] G. Nemethy and H. A. Scheraga, J. Phys. Chem. **66**, 1773 (1962).
[52] G. Nemethy, Angewandte Chemie International Edition in English **6**, 195 (1967).
[53] A. E. Garcia, A. E., G. Hummer, and D. M. Soumpasis, Proteins: Structure, Function, and Bioinformatics **27**, 471 (1997).
[54] D. Paschek, The Journal of Chemical Physics **120**, 6674 (2004).
[55] C. L. Dias, T. Hynninen, T. Ala-Nissila, A. S. Foster, and M. Karttunen, The Journal of Chemical Physics **134**, 065106 (2011).
[56] S. Shimizu and H. S. Chan, The Journal of Chemical Physics **113**, 4683 (2000).
[57] C. Dias and H. S. Chan, (to be submitted). (2012).
[58] G. Panick, H. Herberhold, Z. Sun, and R. Winter, Spectroscopy: An International Journal **17**, 367 (2003).
[59] F. Meersman, L. Smeller, and K. Heremans, Biophysical Journal **82**, 2635 (2002).
[60] A. Ben-Naim, *Water and Aqueous Solution* (Plenum, New York, 1974).
[61] K. A. T. Silverstein, A. D. J. Haymet, and K. A. Dill, J. Am. Chem. Soc. **120**, 3166 (1998).
[62] A. Ben-Naim, J. Chem. Phys. **54**, 3682 (1971).
[63] N. T. Southall and K. A. Dill, Biophys. Chem. **101-102**, 295 (2002).
[64] K. A. Dill, T. M. Truskett, V. Vlachy, and B. Hribar-Lee,

Annu. Rev. Biophys. Biomol. Struct. **34**, 173 (2005).
[65] J. Becker and O. Collet, J. Mol. Struct.: THEOCHEM **774**, 23 (2006).
[66] C. L. Dias, T. Ala-Nissila, M. Grant, and M. Karttunen, Journal of Chemical Physics **131**, 054505 (2009).
[67] T. Hynninen, C. Dias, A. Mkrtchyan, V. Heinonen, M. Karttunen, A. Foster, and T. Ala-Nissila, Computer Physics Communications **183**, 363 (2012).
[68] T. Hynninen, V. Heinonen, C. L. Dias, M. Karttunen, A. S. Foster, and T. Ala-Nissila, Physical Review Letters **105**, 086102 (2010).
[69] A. Bizjak, T. Urbic, V. Vlachy, and K. A. Dill, Acta Chim. Slov. **54**, 532 (2007).
[70] A. Rahman and F. H. Stillinger, J. Chem. Phys. **55**, 3336 (1971).
[71] M. Allen and D. Tildesley, *Computer Simulations of Liquids* (Clarendon, Oxford, 1990).
[72] A. Kolb and B. Dünweg, J. Chem. Phys. **111**, 4453 (1999).
[73] D. Paschek, S. Nonn, and A. Geiger, Phys. Chem. Chem. Phys. **7**, 2780 (2005).
[74] An increase in the temperature of maximum stability with increasing pressure is consistent with the behavior of real proteins for which the slope of this increase is proportional to $\Delta\alpha/\Delta C_{\rm p} > 0$, where $\Delta C_{\rm p}$ and $\Delta\alpha$ are differences in the heat capacity and the thermal expansion coefficient between folded and unfolded states of the protein [75].
[75] S. Laszlo, Biochimica et Biophysica Acta (BBA) - Protein Structure and Molecular Enzymology **1595**, 11 (2002).
[76] H. Flyvbjerg and H. G. Petersen, The Journal of Chemical Physics **91**, 461 (1989).
[77] G. Voronoi, Journal fur die Reine und Angewandte Mathematik **133**, 97 (1907).
[78] L. R. Pratt and D. Chandler, J. Chem. Phys. **67**, 3683 (1977).
[79] See Supplemental Material at [URL will be inserted by publisher] for the PMF of a methane dimer in TIP4P water models and additional simulations highlighting the role of ssc in β-sheet and α-helix.